

Robust Deep Multi-modal Learning Based on Gated Information Fusion Network

Jaekyum Kim¹, Junho Koh¹, Yecheol Kim¹, Jaehyung Choi², Youngbae Hwang³, Jun Won Choi¹

Hanyang University¹, Phantom AI Inc.², KETI³

Abstract. The goal of multi-modal learning is to use complimentary information on the relevant task provided by the multiple modalities to achieve reliable and robust performance. Recently, deep learning has led significant improvement in multi-modal learning by allowing for the information fusion in the intermediate feature levels. This paper addresses a problem of designing robust deep multi-modal learning architecture in the presence of imperfect modalities. We introduce deep fusion architecture for object detection which processes each modality using the separate convolutional neural network (CNN) and constructs the joint feature map by combining the intermediate features from the CNNs. In order to facilitate the robustness to the degraded modalities, we employ the gated information fusion (GIF) network which weights the contribution from each modality according to the input feature maps to be fused. The weights are determined through the convolutional layers followed by a sigmoid function and trained along with the information fusion network in an end-to-end fashion. Our experiments show that the proposed GIF network offers the additional architectural flexibility to achieve robust performance in handling some degraded modalities, and show a significant performance improvement based on Single Shot Detector (SSD) for KITTI dataset using the proposed fusion network and data augmentation schemes.

1 Introduction

Multi-modal learning refers to a machine learning task aiming to improve learning performance using the experience obtained from the different types of multiple data examples. Basically, such multi-modal data delivers rich and diverse information on the phenomenon relevant to the given task. Human is naturally born to be a good multi-modal learner in that it effectively learns from various modalities including audio, video, smell, touch, etc. Among various multi-modal learning tasks, multi-modal fusion has been one of the most challenging problems in machine learning field due to the difficulty of combining the information delivered by the multi-modal sources. Traditionally, multi-modal fusion concerns in which data processing stage the information fusion is conducted, which leads to the categorization into *early fusion* and *late fusion*. While the early fusion aims to extract the joint representation directly from the raw or preprocessed data,

the late fusion aggregates the decisions made by the machine learning models for each modality. The late fusion is considered to be easy to implement but its performance is limited in that the correlation structure existing in multi-modal sources is not fully utilized. Early fusion is also difficult to find a good joint representation due to significantly different data formats and distinct distributions between modalities. Recent emergence of deep neural network (DNN) technique (called deep learning) [1] has enabled the extraction of the hierarchical semantic features from the raw data, and consequently led to better and flexible use of feature-level data fusion. The common practice for such *intermediate fusion* is to construct the shared representation through a pipeline of fusion layers that merge the features obtained by processing each modality. Leveraging the shared representation found by DNN, the multi-modal learning technique, termed deep multi-modal learning (DML), was shown to achieve remarkable performance for a variety of multi-modal learning problems including audio-visual speech recognition [2, 3], multi-modal activity and emotion recognition [4–6], image analysis from RGBD data [7–9], and camera and Lidar sensor fusion [10, 11].

Basically, the ultimate goal of multi-modal learning is to achieve the highest extent of reliability and robustness in performing the given task using the redundant information provided by multi-modal data. This implies that when the information provided by a single modality is not sufficiently good enough, the multi-modal learning uses the complimentary information delivered by the other modalities to compensate for performance loss. The robustness against degraded data quality can also be readily offered by the conventional late fusion approaches which aggregate the decisions in proportion to their credibility which would be a result of processing each modality. On the contrary, it is not obvious how the intermediate fusion for DML can enjoy such selective information combining since it is difficult for the machine to judge the reliability of the intermediate features. One conceivable approach is to train the fusion network with the data set containing various types of degraded examples, hoping that the architecture learns to use only reliable features for multi-modal fusion. However, our empirical evaluation reveals that the existing fusion architectures are not flexible enough to adapt their fusion strategy to the changes in data quality. This requests the design of the new architecture for DML, which can collect the information as needed from each modality accounting for the quality of the intermediate features.

This paper proposes the novel DML architecture that can offer robust performance for missing or degraded modalities. Towards this end, we introduce a feature-level gated information fusion (GIF) network which combines the features obtained for each modality in a way that only information relevant to the task is aggregated. The GIF network controls the amount of information flow incoming from each modality through *gating mechanism*. Specifically, the GIF network selectively gates the contribution of the features by weighting each element of features by the factor between 0 and 1. These weights are independently calculated through the separate network called weight generation (WG) network. The WG network takes all concatenated features for all modalities as an input

and induces the weights to be adjusted such that the given task is properly executed. In fact, this operation resembles the gating operations used in long short term memory (LSTM) [12] in that it controls the operation of information gating in a data-dependent manner. Through the GIF network, we intend to provide the architectural flexibility for giving more credits for the features more relevant to the task. Next, we build the deep 2D object detection architecture based on the proposed multi-modal fusion technique. We first apply the multiple convolutional neural network (CNN) networks (e.g. VGG [13], ResNet [14], etc) to generate the intermediate feature maps for each modality. We combine these feature maps across the modalities through the proposed GIF network, producing the joint feature maps to be used for perform object detection. The procedure for subsequent object detection steps follows that of the current state of the art object detector, single shot detector (SSD) [15].

The key contributions of our work are highlighted below.

- We propose a novel feature-level information fusion scheme which promises robust performance to imperfect modalities. To our best knowledge, such weighted information fusion, which mimics the gating operation of LSTM, has not been utilized for robust feature-level fusion.
- We present the robust 2D object detector built upon the proposed scheme. Note that deep multi-modal fusion is not available for the state of the art detectors (e.g. SSD) yet. Note also that the idea of our weighted information fusion is not limited to the these types of detector and can readily extended to other multi-modal fusion applications.
- In order to promote robustness of our scheme, we train our model using special data augmentation where additional examples are generated by corrupting some of modalities (e.g. blanking, noise addition, occlusion, severe change in illumination). The experiments conducted with the SUN-RGBD dataset [16] and KITTI camera and Lidar dataset [17] show that the proposed architecture achieves better detection accuracy than the existing object detectors especially when some modalities are corrupted. We also show the significantly improved performance based on SSD for generic KITTI dataset using the proposed fusion network and data augmentation schemes.

The rest of the paper is organized as follows. In Section 2, we will review the previous works on the DML. In Section 3, we present the details on the proposed GIF network and the 2D object detector. The experimental results will be provided in Section 4 and the paper will be concluded in Section 5.

2 Related works

In this section, we briefly review the existing works on the DML methods. Then, we introduce the previous deep learning-based objection detectors and their extension to the multi-modal setup.

2.1 Deep Multi-modal Learning

The earliest research on DML goes back to the works showing that the effective joint data representation can be found using deep models such as deep autoencoder [18] and deep Boltzman machine (DBM) [19]. Since then, different structures of DML technique has been realized for a variety of learning tasks including representation learning, data fusion, translation, alignment, etc. (See [20] and [21] for comprehensive review on DML.) Among them, we specifically review the subject of multi-modal fusion due to the relevance to our work. The multi-modal fusion aims to extract as much relevant information on the task as possible from the data having heterogeneous characteristics. Since the emerging DNN produces high-level semantic features through the hierarchical pipelined data processing, the *feature-level fusion*, which combines the features found at the intermediate layers of the DNN, has given rise to an effective means to multi-modal learning.

Thus far, various DML techniques have been proposed for different types of modalities. It has been shown in [2, 5, 6, 18] that the learning performance can be greatly improved using both audio and video data. In [18], the speech recognition was enhanced by using the joint data representation learned from the voice record and the video of lip movement. In [6], the audio feature from CNN and the visual features from the deep belief network were aggregated into single video descriptor for emotion recognition. In [2] and [5], the feature-level multi-modal fusion was shown to achieve good performance in the application to speech recognition and sentiment analysis, respectively. The DML architecture was also designed to generate the effective features for RGB-D (RGB-depth) and multi-view images. In [7], the feature vectors obtained at the fully connected (FC) layer of two separate CNNs were combined to generate the joint features form the RGB-D image. In [8], the performance of the RGB-D fusion was improved by finding the effective encoding scheme for depth image and in [22], the RGB and depth features were projected on the space maximizing the discriminative power in efforts to find the better joint features. In [23], the residual learning structure was proposed to learn multi-modal features for semantic segmentation.

2.2 Object Detection Using Multi-modal Data

Recently, the CNN led to remarkable performance improvement for the recognition of 2D image. Each layer of the CNN applies a series of operations including 2D convolution, pooling, and nonlinear operations to abstract the complex structure of the image at each layer. So far, various CNN architectures have been proposed including VGG, GoogleNet, and ResNet. In the early phase of deep learning, CNN has been exclusively used for image classification but now the CNN is widely used as a backbone network to provide the feature maps for performing more complicated tasks. In this case, the pretrained CNN network is plugged for initialization and the whole system is trained for fine-tuning in an end-to-end fashion.

Thus far, various CNN-based object detectors have been proposed. Basically, these object detectors calculate the score for the bounding box candidate and the object class based on the feature map produced by the CNN. The state-of-the-art object detectors include the faster R-CNN [24], SSD [15], YOLO [25], and YOLOv2 [26]. The object detection can be extended for the multi-modal setup. In [27], object detection based on RGB-D data was performed using the cross-modality feature found by three CNN architectures. In [28], the deep fusion scheme based on RGB-D image was proposed using the *hallucination network* which learns a new RGB image representation by mimicking the depth network. In [10], the multi-view images are constructed from raw Lidar measurement data and used to perform 3D object detection along with RGB image in the context of automated driving. In [11], the authors proposed the *point-fusion network* which predicts the corner location of the 3D bounding box based on the Lidar 3D points.

3 Robust deep multi-modal learning (R-DML)

In this section, we describe our robust deep multi-modal learning (R-DML) architecture and data augmentation method for training the proposed network. The key ingredient of the R-DML is gated information fusion (GIF) network that can adjust the contribution of the feature maps from each modality adaptively based on their quality. Note that the GIF network can be readily applied to various multi-modal learning problems including object detection, segmentation, and recognition tasks. In addition, it can operate well regardless of the number of modalities. The detailed operation of the GIF network will be explained later.

3.1 R-DML Architecture

Overall Architecture The structure of the proposed R-DML is described in Fig. 1. Though our idea can be applied to the case of more than two modalities, we consider the example of two modalities. First, two separate CNN pipelines are used to extract the intermediate features to be fused. Each CNN consists of the CNN backbone network (e.g. VGG-16) and 8 extra convolutional layers. This configuration is similar to that of SSD. We generate the joint features by combining the feature maps at the layers of conv4_3, conv7 (FC7), conv8_2, conv9_2, conv10_2, and conv11_2 layers.¹ These joint feature maps are used to perform object detection in different scales. As shown in Fig. 1, the GIF network is employed for feature-level information fusion. The GIF adjusts the contribution of the feature maps from each modality adaptively, whose detailed operation will be described next. For the purpose of performance evaluation, we also present the baseline object detector called baseline DML (B-DML), which has the same structure as R-DML except that the GIF network is replaced by 1×1 convolution that is used to combine the intermediate features.

¹ We follow the notations of the SSD in [15].

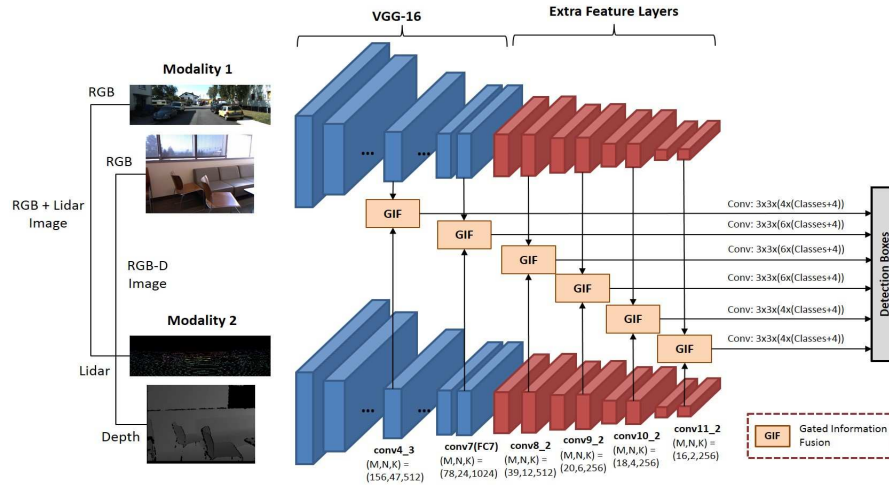


Fig. 1. Overall structure of the proposed R-DML. The R-DML takes the intermediate feature maps from both modality 1 and modality 2 using separate CNNs and combines them through the proposed GIF network. The joint feature maps produced by the GIF network are used to compute the score for object detection following the procedure of SSD.

Gated Information Fusion (GIF) Network Fig. 2 depicts the structure of the GIF network. The GIF network takes the intermediate feature maps from each CNN as an input and performs their weighted fusion. Let \mathbf{F}_1 and \mathbf{F}_2 be the $M \times N \times K$ feature maps obtained by two CNNs corresponding to two input modalities. The actual values of M , N and K for each layer are provided in Fig. 2. The GIF network consists of two parts: 1) information fusion network and 2) WG (Weight Generation) network. The information fusion network multiplies the $M \times N$ weight maps \mathbf{w}_1 and \mathbf{w}_2 to the feature maps \mathbf{F}_1 and \mathbf{F}_2 , respectively. Such multiplication is done in element-wise for each feature map. Then, the weighted feature maps are concatenated across all modalities and $1 \times 1 \times 2K$ convolution is applied to combine the feature maps. These operations result in the joint feature maps \mathbf{F}_J . Meanwhile, the WG network calculates the weights through the separate network based on the input features. After concatenating the feature maps over all modalities, two separate $3 \times 3 \times 1$ CNN kernels \mathbf{C}_1 and \mathbf{C}_2 are applied in parallel. Then, the sigmoid function is applied to produce the weight maps \mathbf{w}_1 and \mathbf{w}_2 . Since the input features are already in sufficiently high abstraction levels, adding additional convolutional layers for the WG network did not help the effectiveness of the gating operation. We summarize the operation of the GIF network in the following equations.

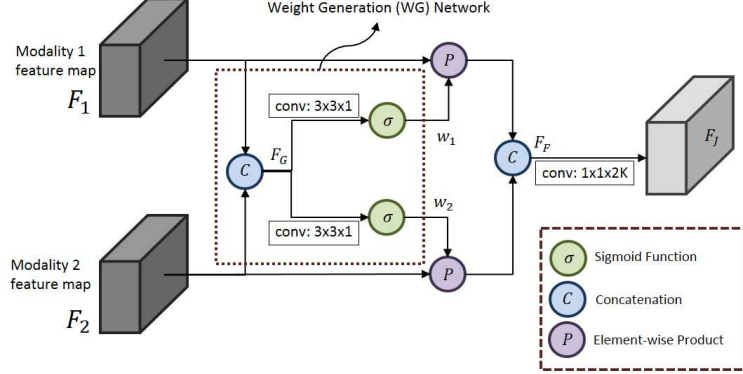


Fig. 2. The structure of the proposed GIF network. The GIF network produces the weight maps \mathbf{w}_1 and \mathbf{w}_2 by applying the convolutional layer and sigmoid function to the input features. Then, \mathbf{w}_1 and \mathbf{w}_2 are multiplied to the feature maps \mathbf{F}_1 and \mathbf{F}_2 for weighted information fusion.

$$\mathbf{F}_G = \mathbf{F}_1 \boxplus \mathbf{F}_2 \tag{1}$$

$$\mathbf{w}_1 = \sigma(\mathbf{C}_1 * \mathbf{F}_G + \mathbf{b}_1) \tag{2}$$

$$\mathbf{w}_2 = \sigma(\mathbf{C}_2 * \mathbf{F}_G + \mathbf{b}_2) \tag{3}$$

$$\mathbf{F}_F(i) = (\mathbf{F}_1(i) \odot \mathbf{w}_1) \boxplus (\mathbf{F}_2(i) \odot \mathbf{w}_2), \quad i = 1, \dots, K, \tag{4}$$

$$\mathbf{F}_J = \text{ReLU}(\mathbf{C}_J * \mathbf{F}_F + \mathbf{b}_F) \tag{5}$$

where

- $\sigma(x) \triangleq \frac{1}{1+e^{-x}}$: sigmoid function(element-wise)
- $x * y$: convolutional layer
- $x \odot y$: element-wise product
- $x \boxplus y$: concatenation
- $\mathbf{F}(i)$: i th feature map of \mathbf{F}
- $\mathbf{b}_F, \mathbf{b}_1, \mathbf{b}_2$: biases of the convolution layers.

3.2 Training

Data Augmentation The goal of the proposed gated fusion is to combine the feature maps appropriately depending on their quality. In order to make our network to learn such robust behavior, we devise the new data augmentation method where the dataset is augmented with the examples created by applying adverse operations to some of modalities. With training examples which includes some corrupted modalities, our model would learn to weight more on the information from the modalities of better quality. The various type of modifications can be applied for data augmentation and the specific types considered in our experiments are provided below:

- Blank Data (Type 1): we feed all pixel value to zero.
- Random occlusion (Type 2): we occlude the object using the black box whose size and location are randomly chosen.
- Severe illumination change (Type 3): we brighten the image in the rounded local region where the center and radius of the region and the brightness are randomly chosen.
- Additive random noise (Type 4): we add the random Gaussian noise where noise variance is randomly chosen within the certain range.
- No action.

Once the type of operation is determined, we randomly choose which modality is subject to the degradation with equal probability.

Training Setup Except for our data augmentation strategy, the training setup used in SSD are adopted for our method including matching strategy, hard negative mining, and multi-task loss function. We use a VGG-16 pretrained model on ImageNet in two parallel CNN pipelines. Stochastic gradient descent (SGD) are used with the mini-batch size of 2. We set the initial learning rate to 0.0005 and the weight decay to 0.0005 for L2 regularization and the momentum of the parameter 0.9. We use the same training setup for KITTI and SUN-RGBD datasets. A total of 130 epochs and 200 epochs are run with the KITTI dataset and SUN-RGBD dataset, respectively.

4 Experimental results

In this section, we evaluate the performance of the proposed R-DML scheme using two public datasets: KITTI dataset [17] and SUN-RGBD dataset [16]. We investigate the behavior of the gating operation to verify the effectiveness of the GIF network. We also compare the performance of our scheme with that of other multi-modal fusion schemes. Note that for fair comparison, we re-trained other algorithms using the same augmentation method as that used to train the R-DML.

4.1 Datasets

KITTI Dataset The KITTI dataset is collected in urban driving scenarios with Pointgrey cameras and a Velodyne HDL-64E Lidar. The training set and test set contain 7,481 images and 7,518 images, respectively. Since the labels of the test images are not publicly available, we split the labeled training dataset into the training set and validation set by half for performance evaluation as in [29]. We evaluate the 2D detection performance with three object categories, i.e., car, pedestrian, and cyclist and three difficult levels, i.e., easy, moderate, hard as proposed in the KITTI Benchmark.

We consider multi-modal fusion task which performs object detection using both RGB image and 3D lidar data. In order to format the data for our object

detector, we convert the 3D point cloud data into the 2D image in camera plane. The 3D point clouds in KITTI dataset contains the 3D coordinate (X, Y, Z) and the reflectivity R measured for each reflected laser pulse. Specifically, we map the 3D coordinate (X, Y, Z) of Lidar data into the 2D coordinate (x, y) on camera plane using

$$\begin{bmatrix} x \\ y \end{bmatrix} = \text{calib_matrix} \cdot \begin{bmatrix} X \\ Y \\ Z \end{bmatrix}. \quad (6)$$

where *calib_matrix* is the matrix for coordinate transformation. Note that we quantize (x, y) to the nearest integer and limit the maximum range of (x, y) by that of camera plane. For the given 2D coordinate (x, y) , we create three channel image by encoding the values of X , Z , and R to the pixel values. This creates the image with the depth, height, and intensity (DHI) channels. The pixel values for the DHI channels are obtained by

$$\text{val}_d = 255 \cdot (1 - \min[X/\text{max}_X, 1]) \quad (7)$$

$$\text{val}_h = 255 \cdot (1 - \min[Z/\text{max}_Z, 1]) \quad (8)$$

$$\text{val}_i = 255 \cdot (1 - \min[R/\text{max}_R, 1]). \quad (9)$$

Note that $X \in [0, \text{max}_X]$, $Z \in [0, \text{max}_Z]$, and $R \in [0, \text{max}_R]$ are mapped to the pixel values between $[0, 255]$ in a linear scale. For example, we set max_X , max_Z , and max_R to 80 meter, 6 meter, and 0.7. Note that such DHI Lidar image and the RGB camera image are treated as two modalities and used as an input to the multi-modal object detectors. We apply data augmentation to these two multi-modal images. Since it is hard to introduce noise and illumination change to the Lidar image, we apply them only for RGB image.

SUN-RGBD Dataset The SUN-RGBD dataset is a large-scale RGB-D dataset collected in indoor environments. It contains the 10,335 RGB-D image pairs that includes NYUDv2 depth [30], Berkeley B3DO [31], and SUN3D [32]. The dataset consists of 5,285 training set and 5,250 testing set. We evaluate the detection performance with 19 object categories as in [16]. Note that we apply the same data augmentation strategy used for the KITTI dataset to this dataset. The examples of the modifications applied to the RGB camera image in SUN-RGBD dataset are illustrated in Fig. 3.

Extended Test Dataset To evaluate the robustness of the proposed R-DML, we randomly generate the test dataset using the same data modification applied to the proposed data augmentation. Both KITTI and SUN-RGBD datasets contain the RGB camera image and the modality 2 corresponds to the Lidar image and depth image, respectively. In our experiments, we come up with the following test cases:

- Total: Test with all normal and degraded examples together.



Fig. 3. Examples of modifications applied to the camera image on SUN-RGBD dataset.

- RGB+modality2: Test with the normal test examples without any degradation.
- RGB (blank)+modality2: Test with the test examples with RGB image blanked.
- RGB+modality2 (blank): Test with the test examples with modality 2 blanked.
- RGB (occlusion)+modality2: Test with the test examples with RGB image occluded.
- RGB+modality2 (occlusion): Test with the test examples with modality 2 occluded.
- RGB (noise)+modality2 : Test with the test examples with the noise of the RGB image changed.
- RGB (illumination)+modality2 : Test with the test examples with the illumination of the RGB image changed.

Note that for our performance evaluation, we used the same number of test examples for each test case.

4.2 Experimental Results on KITTI Dataset

First, we evaluate the performance of the proposed method when tested on KITTI dataset. As a baseline algorithm, the following multi-modal fusion methods are considered:

- B-DML: It has the same structure with R-DML except that both gating weights applied to two modalities are fixed to one.

Table 1. Detection performance (AP) for car category on the extended KITTI test dataset

Test Input	Our R-DML			B-DML			SSD-based fusion [15]			AVOD [33]		
	Easy	Mod.	Hard	Easy	Mod.	Hard	Easy	Mod.	Hard	Easy	Mod.	Hard
Total	93.95	86.70	78.05	89.86	82.21	72.21	89.69	82.03	72.96	-	-	-
RGB + Lidar	98.69	90.31	82.16	93.61	87.01	77.52	91.72	87.93	78.46	89.85	87.99	80.27
RGB (blank) + Lidar	88.86	78.12	69.68	86.56	74.30	64.71	87.92	77.83	69.11	86.42	69.82	69.77
RGB + Lidar (blank)	97.39	90.29	81.84	91.88	88.10	78.68	93.31	89.27	80.03	-	-	-
RGB (occlusion) + Lidar	89.88	88.12	79.03	88.12	78.52	68.85	91.78	88.22	78.80	87.94	78.75	78.53
RGB + Lidar (occlusion)	97.72	90.23	81.94	92.75	87.10	77.67	84.80	74.88	66.33	-	-	-
RGB (noise) Lidar	89.33	80.15	71.12	86.75	75.13	65.71	88.67	76.12	67.18	88.88	79.79	79.46
RGB (illumination) + Lidar	95.82	89.71	80.58	89.37	85.31	75.87	89.69	79.96	70.82	88.60	79.33	79.00

Table 2. Detection performance (AP) for car category on the extended KITTI test dataset with unseen types of perturbation

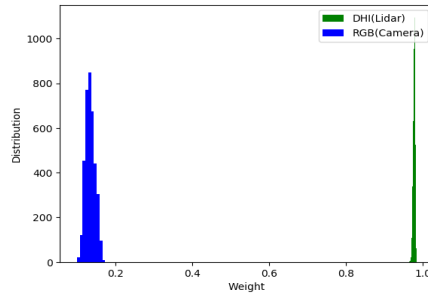
Test Input	Our R-DML			B-DML		
	Easy	Mod.	Hard	Easy	Mod.	Hard
RGB + Lidar (Type1. blank)	-	-	-	-	-	-
RGB + Lidar (Type2. occl.)	83.31	82.23	74.41	80.50	77.37	68.89
RGB + Lidar (Type3. illum.)	90.62	89.06	80.04	89.70	87.22	78.59
RGB + Lidar (Type4. noise)	83.10	73.34	65.67	78.15	66.52	58.25

- SSD-based fusion: We take the late fusion approach based on the final results reported by two SSDs separately trained with the camera and Lidar images. We combine the detection boxes found by two SSDs using non-maximum suppression.
- AVOD [33]: This is the state-of-the-art multi-modal object detection algorithm using both camera and Lidar data. Note that AVOD uses the Lidar top-view image instead of front-view image that we use for our method. Hence, we could not include the RGB + Lidar (occlusion) and RGB + Lidar (blank) cases for training and test.

Table 1 provides the average precision (AP) achieved by the algorithms of interest for *Car* category. The proposed data augmentation strategy is used for training all methods considered. The AP is evaluated using 3,740 test examples for each scenario. We observe that the proposed R-DML shows better detection accuracy than other algorithms in almost all cases. In particular, the R-DML significantly outperforms the B-DML, which shows the benefit of the proposed gated fusion method. We see that the performance gain of the R-DML over B-DML can go up to 5% of AP for some test scenarios (e.g. occlusion case). Interestingly, the proposed scheme outperforms the B-DML even when the normal KITTI data is used without any data corruption for test. Since this KITTI dataset might contain some natural but somewhat benign level of perturbation (e.g. camera noise and adverse illumination change), this could be a part of evidence showing that the R-DML is robust to real world perturbation as well as synthetic one. In essence, all these results show that the proposed GIF network provides better model flexibility to improve the robustness of the algorithm.

Table 3. Detection performance (AP) on KITTI validation set. (*: trained by us, red text: ranked first, blue text: ranked second, green text: ranked third)

Method	Data	Easy	Moderate	Hard
SSD* [15]	Mono	93.31	89.27	80.03
3DOP [29]	Stereo	94.49	89.65	80.97
Mono3D [34]	Mono	95.75	90.01	80.66
Deep Manta [35]	Mono	97.58	90.89	82.72
MV3D [10]	Lidar+Mono	95.01	87.59	79.90
SSD-based fusion*	Lidar+Mono	91.72	87.93	78.46
B-DML*	Lidar+Mono	93.61	87.01	77.52
Our R-DML*	Lidar+Mono	98.69	90.31	82.16

**Fig. 4.** The histogram of the averaged GIF weights at conv4_3 layer. The weights for the blanked data are close to zero. This demonstrates the operation for reducing the contribution from unreliable data.

We evaluate the detection performance on *Pedestrian* and *Cyclist* categories as well. We obtain 70.59 (R-DML) versus 68.37 (B-DML) for moderate level for the pedestrian category and 70.11 (R-DML) versus 68.90 (B-DML) for the cyclist category. The whole results are provided in the supplemental material.

In Table 1, we test the algorithms with the types of perturbation used in the training stage. However, the sorts of perturbation seen in the real world is unpredictable and impossible to be generated. Hence, we evaluate the robustness of the proposed scheme with the unseen types of perturbation. Table 2 provides the performance of the R-DML and B-DML when we train them using the type 1 to $(i - 1)$ perturbation (including normal dataset) and test them with the type i perturbation. For example, the models trained with the dataset corrupted by the type 1 and type 2 perturbations are tested with the type 3 perturbation. Table 2 shows that the R-DML achieves the performance gain over the B-DML for the perturbation types not used for training. These results show that the proposed fusion method exhibits the robust behavior even against unseen perturbation structures.

Next, we look into the behavior of the gating operation in details. Fig. 4 shows the histogram of the GIF weights (averaged over the whole weight map at the conv4_3 layer) for the case that the RGB image is completely blanked. Note that the weights multiplied to the RGB features are close to zero in order

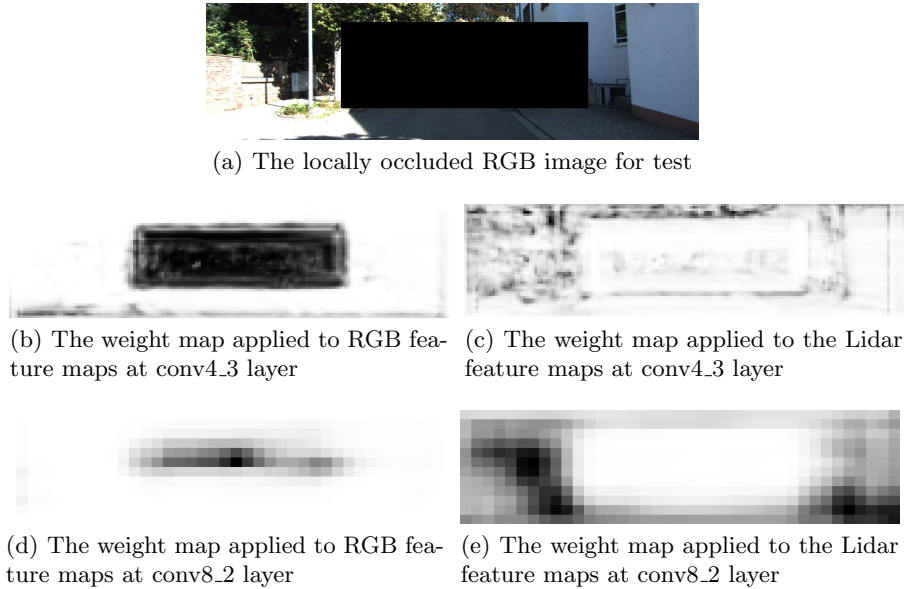


Fig. 5. The visualization of the GFU weight maps at conv4.3 layer and conv8.2 layer. Note that the weights for the RGB features are reduced significantly for the occluded region. This shows that the gating operation conducts locally controlled information fusion.

to reduce the contribution from the blanked data. On the contrary, we see that the weights for the normal Lidar image are close to one. In Fig. 5, we visualize the GIF weight maps learned by the GIF for the case where the RGB image is locally occluded by the black box. We find that the GIF weights in the camera side are small only within the locally occluded region while they are high for the rest of area. Note that the GIF weights for the Lidar image are relatively high for the whole region. This shows our gating mechanism controls the amount of information combined depending on the quality of the features for each interested region.

In Table 3, we compare the performance of the proposed method with other state of the art 2D object detectors. The candidate detectors include SSD [15], 3DOP [29], Mono3D [34], Deep Manta [35], and MV3D [10]. For fair comparison, we use the same train/validation split method used in [10, 29, 34, 35]. Note that SSD-based fusion, B-DML and the proposed R-DML are trained with the proposed data augmentation schemes. We observe that the performance of the proposed object detector is better or on par with the other algorithms for all difficulty levels. This shows that the proposed fusion method exhibits competitive performance and optimal fusion while promising the robust performance even in the adverse environments. Note that even though the proposed R-DML

Table 4. Results for detection performance (mAP) on extended SUN-RGBD test dataset

Test Input	Our R-DML	B-DML	Supervision transfer [9]
Total	34.72	29.13	21.35
RGB + depth	40.43	36.31	26.68
RGB (blank) + depth	30.76	28.37	15.81
RGB + depth (blank)	32.69	12.03	22.25
RGB (occlusion) + depth	35.65	29.39	22.95
RGB + depth (occlusion)	35.04	33.12	22.75
RGB (noise) + depth	32.76	31.50	16.65
RGB (illumination) + depth	35.67	33.19	22.40

is built upon the baseline SSD, significant performance gain is achieved over the baseline SSD through the multi-modal fusion strategy proposed in our work.

4.3 Experimental Results on SUN-RGBD Dataset

Table 4 provides the mean average precision (mAP) of the proposed object detection algorithm. Since there are not many recent 2D object detection algorithms using SUN-RGBD dataset, we compare our method with only the B-DML and supervision transfer (ST) methods [9]. The ST method is the fast-RCNN [36] based object detector which combines the detection boxes obtained by two separate object detectors. For fair comparison, we trained the B-DML and ST with the same augmentation method as that used for our R-DML. For each test case, we use the 5,250 test examples. We see in Table 4 that the proposed R-DML achieves better detection accuracy than the B-DML, which reveals the effectiveness of our gated fusion algorithm for the task of the RGB-D fusion as well. Note that the R-DML maintains the performance gain over the B-DML even when the normal SUN-RGBD dataset are used for test without any modification. The AP results per category are provided in supplemental material.

5 Conclusions

In this paper, we proposed the robust multi-modal learning technique which fuses the intermediate features produced by the CNN with appropriate contributions. Inspired by the gating mechanism used in LSTM, we devised the gated information fusion network, which combines the features from each modality with the weights computed based on the input features to be fused. Such GIF network was used to perform 2D object detection using multi-modal inputs and the whole system is trained end-to-end. We used the special data augmentation strategy for promoting the robustness of our system, which corrupts some of modalities using various artificial operations. The experiments performed over KITTI dataset and SUR-RGBD dataset shows the superiority of the proposed method for the scenarios of missing or degraded modalities.

References

1. Lecun, Y., Bengio, Y., Hinton, G.: Deep learning. *Nature* **521** (2015) 436–444
2. Mroueh, Y., Marcheret, E., Goel, V.: Deep multimodal learning for audio-visual speech recognition. *Proc. IEEE Int. Conf. on Acous., Speech and Signal Processing (ICASSP)* (2015)
3. Noda, K., Yamaguchi, Y., Nakadai, K., Okuno, H.G., Ogata, T.: Audio-visual speech recognition using deep learning. *Applied Intelligence* **42** (2015) 722–737
4. Radu, V., Lane, N.D., Bhattacharya, S., Mascolo, C., Marina, M.K., Kawsar, F.: Towards multimodal deep learning for activity recognition on mobile devices. In: *Proc. 2016 ACM Inter. Joint Conf. on Pervasive and Ubiquitous Computing*. (2016) 185–188
5. Poria, S., Cambria, E., Gelbukh, A.: Deep convolutional neural network textual features and multiple kernel learning for utterance-level multimodal sentiment analysis. In: *Proc. Conf. Empirical Methods in Natural Lang. Process.* (2015) 2539–3544
6. Kahou, S.E., Bouthillier, X., Lamblin, P., Gülehdre, C., Michalski, V., Konda, K.R., Jean, S., Froumenty, P., Dauphin, Y., Boulanger-Lewandowski, N., Ferrari, R.C., Mirza, M., Warde-Farley, D., Courville, A.C., Vincent, P., Memisevic, R., Pal, C.J., Bengio, Y.: Emonets: Multimodal deep learning approaches for emotion recognition in video. *Journal on Multimodal User Interfaces* **10** (2015) 99–111
7. Eitel, A., Springenberg, J.T., Spinello, L., Riedmiller, M.A., Burgard, W.: Multimodal deep learning for robust rgb-d object recognition. *Proc. IEEE/RSJ Inter. Conf. on Intel. Robots and Syst. (IROS)* (2015)
8. Gupta, S., Girshick, R., Arbeláez, P., Malik, J.: Learning rich features from rgb-d images for object detection and segmentation. In: *Proc. European Conf. on Computer Vision (ECCV)*. (2014)
9. Gupta, S., Hoffman, J., Malik, J.: Cross modal distillation for supervision transfer. In: *Proc. IEEE Conf. on Computer Vision and Pattern Recog. (CVPR)*. (2016)
10. Chen, X., Ma, H., Wan, J., Li, B., Xia, T.: Multi-view 3d object detection network for autonomous driving. In: *Proc. IEEE Conf. on Computer Vision and Pattern Recog. (CVPR)*. (2017)
11. Xu, D., Anguelov, D., Jain, A.: Pointfusion: Deep sensor fusion for 3d bounding box estimation. In: *Proc. IEEE Conf. on Computer Vision and Pattern Recog. (CVPR)*. (2017)
12. Hochreiter, S., Schmidhuber, J.: Long short-term memory. *Neural computation* **9** (1997) 1735–1780
13. Simonyan, K., Zisserman, A.: Very deep convolutional networks for large-scale image recognition. *arXiv preprint arXiv:1409.1556* (2014)
14. He, K., Zhang, X., Ren, S., Sun, J.: Deep residual learning for image recognition. In: *Proc. IEEE Conf. on Computer Vision and Pattern Recog. (CVPR)*. (2016)
15. Liu, W., Anguelov, D., Erhan, D., Szegedy, C., Reed, S., Fu, C.Y., Berg, A.C.: Ssd: single shot multibox detector. In: *Proc. European Conf. on Computer Vision (ECCV)*. (2016)
16. Song, S., Lichtenberg, S.P., Xiao, J.: Sun rgb-d: A rgb-d scene understanding benchmark suite. In: *Proc. IEEE Conf. on Computer Vision and Pattern Recog. (CVPR)*. (2015)
17. Geiger, A., Lenz, P., Urtasun, R.: Are we ready for autonomous driving? the kitti vision benchmark suite. In: *Proc. IEEE Conf. on Computer Vision and Pattern Recog. (CVPR)*. (2012)

18. Ngiam, J., Khosla, A., Kim, M., Nam, J., Lee, H., Ng, A.Y.: Multimodal deep learning. In: Proc. Int. Conf. on Machine Learning (ICML). (2011)
19. Srivastava, N., Salakhutdinov, R.: Multimodal learning with deep boltzmann machines. *Journal of Machine Learning Research* **15** (2014) 2949–2980
20. Baltrušaitis, T., Ahuja, C., Morency, L.P.: Multimodal machine learning: a survey and taxonomy. *IEEE Transactions on Pattern Analysis and Machine Intelligence* (2018)
21. Ramachandram, D., Taylor, G.W.: Deep multimodal learning. *IEEE Signal Processing Magazine* **34** (2017) 96–108
22. Zhu, H., Weibel, J.B., Lu, S.: Discriminative multi-modal feature fusion for rgbd indoor scene recognition. In: Proc. IEEE Conf. on Computer Vision and Pattern Recog. (CVPR). (2016)
23. Park, S.J., Hong, K.S., Lee, S.: Rdfnet: Rgb-d multi-level residual feature fusion for indoor semantic segmentation. In: Proc. IEEE Conf. on Computer Vision and Pattern Recog. (CVPR). (2017)
24. Ren, S., He, K., Girshick, R., Sun, J.: Faster r-cnn: Towards real-time object detection with region proposal networks. In: *Adv. in Neural Information Proc. Syst.* (2015)
25. Redmon, J., Divvala, S., Girshick, R., Farhadi, A.: You only look once: unified, real-time object detection. In: Proc. IEEE Conf. on Computer Vision and Pattern Recog. (CVPR). (2016)
26. Redmon, J., Farhadi, A.: Yolo9000: better, faster, stronger. In: Proc. IEEE Conf. on Computer Vision and Pattern Recog. (CVPR). (2017)
27. Xu, X., Li, Y., Wu, G., Luo, J.: Multi-modal deep feature learning for rgb-d object detection. *Pattern Recognition* **72** (2017) 300–313
28. Hoffman, J., Gupta, S., Darrell, T.: Learning with side information through modality hallucination. In: Proc. IEEE Conf. on Computer Vision and Pattern Recog. (CVPR). (2016)
29. Chen, X., Kundu, K., Zhu, Y., Berneshawi, A.G., Ma, H., Fidler, S., Urtasun, R.: 3d object proposals for accurate object class detection. In: *Adv. in Neural Information Proc. Syst.* (2015)
30. Silberman, N., Hoiem, D., Kohli, P., Fergus, R.: Indoor segmentation and support inference from rgb-d images. In: Proc. European Conf. on Computer Vision (ECCV). (2012)
31. Janoch, A., Karayev, S., Jia, Y., Barron, J.T., Fritz, M., Saenko, K., Darrell, T.: A category-level 3d object dataset: Putting the kinect to work. In: *Consumer Depth Cameras for Computer Vision.* (2013) 141–165
32. Xiao, J., Owens, A., Torralba, A.: Sun3d: A database of big spaces reconstructed using sfm and object labels. In: Proc. IEEE Int. Conf. on Computer Vision (ICCV). (2013)
33. Ku, J., Mozifian, M., Lee, J., Harakeh, A., Waslander, S.: Joint 3d proposal generation and object detection from view aggregation. *arXiv preprint arXiv:1712.02294* (2017)
34. Chen, X., Kundu, K., Zhang, Z., Ma, H., Fidler, S., Urtasun, R.: Monocular 3d object detection for autonomous driving. In: Proc. IEEE Conf. on Computer Vision and Pattern Recog. (CVPR). (2016)
35. Chabot, F., Chaouch, M., Rabarisoa, J., Teulière, C., Chateau, T.: Deep manta: A coarse-to-fine many-task network for joint 2d and 3d vehicle analysis from monocular image. In: Proc. IEEE Conf. Computer Vision Pattern Recog.(CVPR). (2017)
36. Girshick, R.: Fast r-cnn. In: Proc. IEEE Int. Conf. on Computer Vision (ICCV). (2015)